Nonlinear plate vibrations: A modal approach with application to cymbals and gongs

M. Ducceschi[a], C. Touzé[a] and S. Bilbao[b]

[a]UME (Unité de Mécanique), ENSTA - ParisTech, Chemin de la Hunière, 91761 Palaiseau, France
[b]University of Edinburgh, Room 7306B, James Clerk Maxwell Building, King's Buildings, EH9 3JZ Edinburgh, UK
ducceschi@ensta.fr

A von Kármán simply supported plate is considered. A general strategy is developed for the solution of the nonlinear equations: the solution is expanded onto the linear normal modes for the displacement and stress function. To this extent, a general numerical method is devised to deal with cases where no analytical solutions are available. Description of the nonlinear coupling coefficients can then be done in terms of the linear eigenfunctions. The role of these coefficients is shown to be involved in explaining the complicated dynamics of the plate in nonlinear free oscillations. The current model is validated through comparison with other results in the literature and thanks to a finite difference scheme.

1   Introduction

Acoustical interest of rectangular thin plate vibrations resides in their ability to simulate the sound of more realistic percussive instruments such as gongs and cymbals [14]. However, the relatively simpler geometry of rectangular plates allows for a more systematic study than other structures like cymbals or shells. Plates present shimmering and crashing sounds when the amplitude of vibration becomes comparable to the plate thickness, thus violating the basic assumption of linear vibrations. Large vibration patterns can be originated thanks to external forcing, like an impulsive load (for example, by striking the plate with a mallet), or a sinusoidal forcing of reasonable amplitude.

Nonlinear plate vibrations can be described by the von Kármán equations. These take into account a quadratic correction to the longitudinal strain, as compared to the classical linear plate equation by Kirchhoff [12]. The type of nonlinearity introduced is thus purely geometrical.

Due to the vast spectrum of applications, rectangular plates have been the subject of extensive research, with special attention to analytical or numerical models. Amongst others, one could cite the pioneering works of Chu and Herrmann [5] and Yamaki [15], and more recent developments by Seo et al. [11] and Anlas and Elbeyli [2]. Finite elements methods were employed by Ribeiro and Petyt [9, 10], Ribeiro [8], Boumediene et al. [4]. However, very few experiments have been performed. Amabili [1] used a parameter continuation software to perform bifurcation analysis, and compared the results with experimental data, finding satisfactory agreement. In the realm of sound synthesis, Bilbao [3] developed a finite difference scheme to integrate the equations directly in the time domain.

Here, another numerical test is developed. It makes use of a pure modal approach, where the solution is expanded onto the *linear* normal modes for the displacement and stress functions. The modal expansion is truncated at an order N so that the original system is viewed as an N-degree-of-freedom system where the modes interact nonlinearly. The original partial differential equations can be integrated directly in the space coordinates, thus leaving a set of ordinary nonlinear differential equations.

Although the cited works take into account various aspects of nonlinear plate theory and boundary conditions, none of them is really focused on quantifying and explaining the nature of the coupling coefficients. This model then is specifically designed to give a natural description of the coupling coefficients, that, in theory, can be calculated *systematically* for any set of boundary conditions.

The case under study is that of a *simply supported* plate. In the literature, different sets of boundary conditions correspond to the simply supported case. The distinction is originated upon the role that the Airy stress function plays in the in-plane motion. Here, the case of a simply supported plate with *in-plane* movable edges is chosen. The conditions for the transverse motion are then simply given by imposing zero displacement and flexural moments at the boundary. For the in-plane motion with movable edges, one imposes the Airy stress function to vanish along with its first normal derivative, as shown in [12]. As a result, the stress function equation takes the same form as that of a clamped Kirchhoff plate.

The solution for the displacement is given analytically by a double Fourier sine series, which also provides the linear eigenfrequencies. The Airy function case instead does not have an analytical solution. One has then to resort to some numerical strategy. Here the choice was to follow the work by W.L. Li [7], who makes use of the *Rayleigh-Ritz method* by constructing the solution upon a modified double Fourier cosine series.

Once that the linear normal modes are found, one can manipulate the von Kármán system to derive a set of coupled ordinary differential equations with cubic nonlinearities.

The current model is validated by direct comparison with a finite difference scheme by Bilbao [3], as well as previous results found in the literature. Free vibrations are inspected thanks to a continuation software, allowing the computation of the nonlinear amplitude-frequency relations, exhibiting complicated dynamics with numerous internal resonances and coupled branches.

2   Model Description

2.1   Modal Equations

The current section presents the von Kármán equations as well as the modal approach adopted for the resolution. It is assumed that the linear modes are known regardless the particular form of the boundary conditions. A discussion specific to the simply supported case is found in the next sections.

A rectangular plate of dimensions L_x, L_y is considered. The plate is homogeneous, isotropic, of density ρ, Young's modulus E and Poisson's ratio ν. Its *flexural rigidity* is $D = Eh^3/12(1-\nu^2)$. The von Kármán system then reads

$$D\Delta\Delta w + \rho h \ddot{w} + c\dot{w} = L(w,F) + \delta(\mathbf{x}-\mathbf{x_0})f\cos(\Omega t) \quad (1a)$$

$$\Delta\Delta F = -\frac{Eh}{2}L(w,w) \quad (1b)$$

where Δ is the Laplacian operator, $w = w(x,y,t)$ is the transverse displacement and $F = F(x,y,t)$ is Airy stress function. The equations present a viscous damping term $c\dot{w}$ and a sinusoidal forcing term $\delta(\mathbf{x}-\mathbf{x_0})f\cos(\Omega t)$ applied at the point $\mathbf{x_0}$ on the plate. The damping will take the form of *modal* viscous damping once that the equations are discretised along the normal modes. The bilinear operator $L(\cdot,\cdot)$ is known as *von Kármán operator* [12] and, in cartesian coordinates, it

has the form of

$$L(\alpha, \beta) = \alpha_{,xx}\beta_{,yy} + \alpha_{,yy}\beta_{,xx} - 2\alpha_{,xy}\beta_{,xy} \qquad (2)$$

where $_{,s}$ denotes differentiation with respect to the variable s. This operator, although itself bilinear, is the source of the nonlinear terms in the equations. All the quantities are taken in their natural units, so that Eq. (1a) and Eq. (1b) have the dimensions, respectively, of $kg\ m^{-1}\ s^{-2}$ and $kg\ m^{-2}\ s^{-2}$.

The displacement w and the stress function F are then discretised along the linear modes. This is to say that they satisfy the following linear partial differential equations:

$$w = S_w \sum_{k=1}^{\infty} \frac{\Phi_k(x,y)}{\|\Phi_k\|} q_k(t);$$

$$\Delta\Delta\Phi_k(x,y) = \frac{\rho h}{D}\omega_k^2\Phi_k(x,y) \qquad (3a)$$

$$F = S_F \sum_{k=1}^{\infty} \frac{\Psi_k(x,y)}{\|\Psi_k\|} \eta_k(t);$$

$$\Delta\Delta\Psi_k(x,y) = \zeta_k^4\Psi_k(x,y) \qquad (3b)$$

along with the appropriate boundary conditions. A discussion on boundary conditions is found in [12]. The next subsection will deal with the case of a simply supported plate with movable edges. For conciseness, the dependence of the functions on the variables x, y, t will not be displayed any more, unless necessary.

The numbers S_w and S_F are constants of normalisation that can be chosen arbitrarily. They are introduced so that the norms of the functions

$$\bar{\Phi}_k = S_w\frac{\Phi_k}{\|\Phi_k\|}; \qquad \bar{\Psi}_k = S_F\frac{\Psi_k}{\|\Psi_k\|} \qquad (4)$$

are, respectively, S_w and S_F. The linear modes so defined orthogonal with respect to integration over the problem's domain. Orthogonality is intended in the sense of L^2 real function spaces, where the inner product between two members α and β of the space is

$$\langle \alpha, \beta \rangle = \int_S \alpha\beta\ \mathrm{d}S \qquad (5)$$

This allows for manipulation of Eq. (1) when used in combination with Eq. (3). Starting with Eq. (1b), one obtains

$$\eta_k = -\frac{Eh}{2\zeta_k^4}\frac{S_w^2}{S_F}\sum_{p,q} q_p q_q \frac{\int_S \Psi_k L(\Phi_p, \Phi_q)\mathrm{d}S}{\|\Psi_k\|\|\Phi_p\|\|\Phi_q\|} \qquad (6)$$

Integration was performed over the domain S, and the orthogonality relation was used. Eq. (1a) needs a longer manipulation, thus all the steps are presented. First, the displacement and stress functions are written using the modal expansions:

$$\rho h S_w \sum_k \frac{\omega_k^2\Phi_k}{\|\Phi_k\|}q_k + \rho h S_w \sum_k \frac{\Phi_k}{\|\Phi_k\|}\ddot{q}_k + cS_w \sum_k \frac{\Phi_k}{\|\Phi_k\|}\dot{q}_k =$$

$$\sum_{p,n} \frac{S_F S_w}{\|\Psi_n\|\|\Phi_p\|}q_p\eta_n L(\Phi_p, \Psi_n) + \delta(\mathbf{x}-\mathbf{x_0})f\cos(\Omega t) \qquad (7)$$

Then the expression for η_n in Eq. (6) is substituted into Eq. (7) to obtain, on the right hand side

$$\ldots = -\frac{EhS_w^3}{2}\sum_{n,p,q,r}\frac{1}{\zeta_n^4}\frac{L(\Phi_p, \Psi_n)}{\|\Psi_p\|\|\Phi_n\|}\frac{\int_S \Psi_n L(\Phi_q, \Phi_r)\mathrm{d}S}{\|\Phi_q\|\|\Phi_r\|\|\Psi_n\|}q_p q_q q_r$$

$$+\delta(\mathbf{x}-\mathbf{x_0})f\cos(\Omega t) \qquad (8)$$

Now both sides are multiplied by Φ_s, and integrals over the domain are taken:

$$\|\Phi_s\|\rho h S_w(\omega_s^2 q_s + \ddot{q}_s + 2\chi_s\omega_s\dot{q}_s) =$$

$$-\frac{EhS_w^3}{2}\sum_{p,q,r}^n \frac{1}{\zeta_n^4}H_{q,r}^n E_{p,n}^s\|\Phi_s\|q_p q_q q_r + \Phi_s(\mathbf{x_0})f\cos(\Omega t) \qquad (9)$$

Note that, after integration, each one of the modes presents its own modal damping, as defined in [1]. The tensors H and E are:

$$H_{q,r}^n = \frac{\int_S \Psi_n L(\Phi_q, \Phi_r)\mathrm{d}S}{\|\Psi_n\|\|\Phi_q\|\|\Phi_r\|}; E_{p,n}^s = \frac{\int_S \Phi_s L(\Phi_p, \Psi_n)\mathrm{d}S}{\|\Phi_p\|\|\Phi_s\|\|\Psi_n\|} \qquad (10)$$

Both members can be divided by $\|\Phi_s\|\rho h S_w$ to obtain

$$\ddot{q}_s + 2\chi_s\omega_s\dot{q}_s + \omega_s^2 q_s =$$

$$-\frac{ES_w^2}{2\rho}\sum_{p,q,r}^n \frac{H_{q,r}^n E_{p,n}^s}{\zeta_n^4}q_p q_q q_r + \frac{\Phi_s(\mathbf{x_0})}{\|\Phi_s\|\rho h S_w}f\cos(\Omega t) \qquad (11)$$

A fourth order tensor $\Gamma_{p,q,r}^s$ defined as

$$\Gamma_{p,q,r}^s = \sum_n \frac{E}{2\rho}\frac{H_{q,r}^n E_{p,n}^s}{\zeta_n^4} \qquad (12)$$

is introduced in Eq. (11) and represents the tensor of the cubic coupling coefficients.

2.2 Boundary Conditions

The case under study is that of a simply supported plate with movable edges. This translates into the following boundary conditions for Eq. (3a) and Eq. (3b):

$$\Phi_k = \frac{\partial^2\Phi_k}{\partial n^2} = 0\ \forall\mathbf{x}\in\partial S \qquad (13a)$$

$$\Psi_k = \frac{\partial\Psi_k}{\partial n} = 0\ \ \forall\mathbf{x}\in\partial S \qquad (13b)$$

where ∂S is the boundary of the rectangular area S and n indicates the direction normal to the boundary. Eq. (3a) along with conditions (13a) is easily solved by considering

$$\Phi_k(x,y) = X_m^\Phi(x)Y_n^\Phi(y) = \sin\left(\frac{m\pi x}{L_x}\right)\sin\left(\frac{n\pi y}{L_y}\right) \qquad (14)$$

and thus

$$\omega_k^2 = \frac{D}{\rho h}\left[\left(\frac{m\pi}{L_x}\right)^2 + \left(\frac{n\pi}{L_y}\right)^2\right]^2 \qquad (15)$$

Note that the index $_k$ is indeed a double index $_{m,n}$. The modes are sorted in ascending order according to the value of their eigenfrequencies.

The equation for Ψ_k does not present an analytical solution. The next section is then devoted to explaining the numerical model employed to solve the equation.

3 A solution for the clamped plate

Eq. (3b) along with (13b) represents the Kirchhoff linear clamped plate equation. Li [7] presents a method to solve equations of the type (3b) with general boundary conditions. Here however emphasis is put on the clamped case. The

equation of motion and boundary conditions are obtained thanks to a variational approach of the form

$$\delta \int_{t_0}^{t_1} (T - V)\, dt = 0 \qquad (16)$$

for two arbitrary instants t_0, t_1. T and V are the kinetic and potential energies of the system, a form of which reads

$$2V = \int_S \left(F_{,xx}^2 + F_{,yy}^2 + 2\nu F_{,xx} F_{,yy} + 2(1-\nu) F_{,xy}^2 \right)\, dx\,dy \qquad (17)$$

$$2T = \int_S F_{,t}^2\, dx\,dy \qquad (18)$$

For a linear, unforced problem the function F is

$$F = \sum_{k=1}^{M} e^{j\zeta_k^2 t} \Psi_k \qquad (19)$$

The number M is, in theory, infinite; however, for the sake of numerics one needs to perform truncation up to a finite size. Influence of truncation will be briefly shown in the next section.

The function Ψ_k is chosen in the following manner:

$$\Psi_k = \sum_{m,n} d_k^{m,n} X_m^{\Psi}(x) Y_n^{\Psi}(y) \qquad (20)$$

where

$$X_m^{\Psi}(x) = \cos\left(\frac{m\pi x}{L_x}\right) + \sum_{s=0}^{4} a_s x^s \qquad (21a)$$

$$Y_n^{\Psi}(y) = \cos\left(\frac{n\pi y}{L_y}\right) + \sum_{s=0}^{4} b_s y^s \qquad (21b)$$

This represents a double modified Fourier cosine series. The polynomials $\sum_{s=0}^{4} a_s x^s$ and $\sum_{s=0}^{4} b_s y^s$ are chosen so that the boundary conditions (13b) are automatically satisfied. In this sense, a possible solution is

$$\sum_{s=0}^{4} a_s x^s =$$
$$\frac{15(1+(-1)^m)}{L_x^4} x^4 - \frac{4(8+7(-1)^m)}{L_x^3} x^3 + \frac{6(3+2(-1)^m)}{L_x^2} x^2 - 1 \qquad (22)$$

and similarly for $\sum_{s=0}^{4} b_s y^s$. When Eq. (19) and (20) are inserted into (16), one obtains a scalar equation from which an eigenvalue problem can be extracted, i.e.

$$\mathbf{d}^T (\mathbf{K} - \zeta^4 \mathbf{M}) \mathbf{d} = 0; \qquad \mathbf{d}^T = [d_{00}, d_{01}, ..., d_{mn}, ...] \qquad (23)$$

The explicit forms of the matrices $\mathbf{K}$ and $\mathbf{M}$ are rather involved and are not presented here.

Li [7] shows that the modified double cosine series approach remains valid in the case of general elastic support at the edges. This includes all the "classical" boundary conditions plus mixed and intermediate cases. Generally, one imposes the boundary conditions to be satisfied automatically by the displacement function, and then defines an eigenvalue problem of type (23) which produces the eigenfrequencies and the expansion coefficients $\mathbf{d}$.

4 Numerical results

Table 1 presents the clamped plate eigenfrequencies ζ_k obtained by retaining $M = 64$ modes along with those by

Table 1: Comparison of clamped plate frequencies

k	$\zeta_k^2 \cdot L_x L_y$		
	Model	**Leissa**	**FD**
1	40.51	40.51	40.05
2	62.56	62.58	61.93
3	99.19	98.25	98.00
10	208.0	207.9	205.50
20	359.6	-	355.32

Leissa [6], as well those produced by Bilbao's finite differences scheme [3]. The plate parameters are: $L_x = 0.6$ m, $L_y = 0.4$ m, $\rho = 7860$ kg/m^3, $\nu = 0.3$, $h = 0.001$ m, $E = 2 \cdot 10^{11}$ Pa. The FD scheme presents 242×161 discretisation points along the x and y directions, i.e. $dx\,dy/(L_x L_y) = 2.6 \cdot 10^{-5}$. Table 2 gives three nondimensional Gamma coefficients $\Gamma_{k,k,k}^k$ for a plate with the same physical parameters but where $L_x = L_y = 0.3$ m. For this calculation, a total number $M = 81$ of Airy stress function modes was retained in definition (12). The finite difference scheme was run with 121×121 grid points, or $dx\,dy/(L_x L_y) = 6.8 \cdot 10^{-5}$. Table 3

Table 2: Comparison of Gamma coefficients

k	$\Gamma_{k,k,k}^k \cdot \frac{\rho}{E}(L_x L_y)^3$	
	Model	**FD**
1	25.30	25.89
25	$2.071 \cdot 10^4$	$2.141 \cdot 10^4$
50	$7.748 \cdot 10^4$	$7.540 \cdot 10^4$

presents the convergence of the same Γ's for different values of M, calculated using the modal approach. Finally, Table 4 presents the calculation for $\Gamma_{1,1,1}^1$ using the finite difference scheme, and it highlights the effects of truncation for different grid meshes. Numbers in brackets are the average calculation times for a basic MATLAB implementation. Note that, for the modal approach, most of the calculation time goes into the calculation of the norms $\|\Psi_k\|$. Once this is done, the actual calculation of each one of the Γ's is much faster (about 0.1 s for M = 81). Thus, the calculation time per coefficient decreases with the total number of coefficients calculated.

The tables show good agreement between the data for the eigenfrequencies, with discrepancies of the order of a few percents. In addition, the calculation of the Γ's shows the consistency of the modal approach. Convergence up to a desired value can be obtained for each of the Γ's by retaining a sufficient amount of stress function modes.

Table 3: Convergence of Γ's, modal approach

	$\Gamma_{k,k,k}^{k} \cdot \frac{\rho}{E}(L_x L_y)^3$		
M	k = 1	k = 25	k = 50
81	25.30 ($\sim$13s)	$2.071 \cdot 10^4$	$7.748 \cdot 10^4$
144	25.30	$2.078 \cdot 10^4$	$7.761 \cdot 10^4$
256	25.30	$2.100 \cdot 10^4$	$7.922 \cdot 10^4$
324	25.30 ($\sim$750s)	$2.100 \cdot 10^4$	$7.922 \cdot 10^4$

Table 4: Convergence of $\Gamma_{1,1,1}^{1}$, Finite Differences

	$\Gamma_{1,1,1}^{1} \cdot \frac{\rho}{E}(L_x L_y)^3$		
M	Grid pts = 38$\times$38	Grid pts = 86$\times$86	Grid pts = 121$\times$121
49	27.103 ($\sim$1s)	26.117	28.882
64	27.107	26.121 ($\sim$6s)	25.886
81	27.108	26.121	25.886 ($\sim$22s)

5 Free vibrations of nonlinear plate

In this section, the periodic orbits (also called the Non-linear Normal Modes, NNMs) of the simply supported plate are computed, for the first two modes. The plate has got the following physical parameters: $L_x = 0.4$ m, $L_x = 0.6$, $\rho = 7860$ kg/m^3, $\nu = 0.3$, $h = 0.001$ m, $E = 2 \cdot 10^{11}$ Pa. It is the same plate as the one used in [13] for the transition to turbulence. A numerical continuation technique (predictor-corrector with pseudo-arclength continuation, implemented in the software AUTO) is used for this task. The resulting amplitude-frequency plots display the nonlinear dependance of the frequency on the vibration amplitude, and give insight into the nonlinear dynamics of the plates, showing precisely the coupling and energy transfers that can be expected.

Figure 1 shows the result for the first mode, for a model including the first six modes, and up to a vibration amplitude of 6 times the thickness. The main branch, denoted $\mathbf{B}_1$ shows a hardening behaviour, as it is usual for plates: the frequency increases with the amplitudes. For that branch, a strong non-resonant coupling with the fourth is observed, which is due to the presence of a term q_1^3 in the fourth modal equation for q_4. Hence q_4 is present with a noticeable amplitude, that is why on fig. 1, the main branch $\mathbf{B}_1$ is denoted with $\mathbf{B}_1^1$ and $\mathbf{B}_1^4$, the upper index indicating the modal coordinate involved. For $\omega=1.13\omega_1$, an instability occurs for the main branch $\mathbf{B}_1^1$, and a resonant coupling with the second mode appears, resulting in the coupled $\mathbf{B}_{12}$ branch. A 1:3 internal resonance is here at hand, and branch $\mathbf{B}_{12}^2$ starts from zero up to an important amplitude. Following further the main branch $\mathbf{B}_1$, new coupled solutions are found around $\omega \simeq 1.5\omega_1$, and for a vibration amplitude of four times the thickness. The resonant coupling involves mainly the sixth mode, thus the branch is

Figure 1: Frequency-amplitude dependence of the first mode of the selected plate. Maximum of modal coordinates q_i is plotted as a function of the normalised frequency ω/ω_1. q_1 in blue, q_2 in red, q_3 in magenta, q_4 in green, q_5 in orange and q_6 in brown. Unstable states are displayed in a dotted line.

denoted as $\mathbf{B}_{16}$. The resonant coordinate is the sixth one, $\mathbf{B}_{16}^6$, and interestingly enough the sixth mode is coupled via a non-resonant term of the form q_6^3 with the third coordinate, which also appears in the plot, see $\mathbf{B}_{16}^3$. Finally a coupled branch with mode 5, $\mathbf{B}_{15}$, is also observed, but mainly leads to unstable solutions.

The amplitude-frequency relationship for the second mode is shown in Fig. 2. The retained model contains now the first eight modes. Once again, the main branch $\mathbf{B}_2$ shows a hardening behaviour, and a non-resonant coupling with the seventh mode is noticeable ($\mathbf{B}_2^7$). Internal resonances lead to tongues of coupled states, with the fifth mode, $\mathbf{B}_{25}$, and then with the eighth mode, $\mathbf{B}_{28}$. The eighth mode is also non-resonantly coupled with modes 1 and 4, which appears in the branch $\mathbf{B}_{28}$.

6 Conclusion

A general modal approach for nonlinear plates was presented. The particular case of a simply supported plate was taken under consideration. To this extent, a numerical solution strategy to compute the stress function was used, and the results were compared with similar results in the literature and with a finite difference scheme, finding consistent agreement. A few nonlinear coupling coefficients were calculated and their convergence was shown. Finally, bifurcation diagrams for free vibrations of the first two modes were plotted, and the internal resonances were explained in light of the specific weight of each of the coupling coefficients in the equations of motion. This model can serve as a basis for various applications: sound synthesis of gong-like instruments, nonlinear dynamics of a multi-degree-of-freedom system, in-
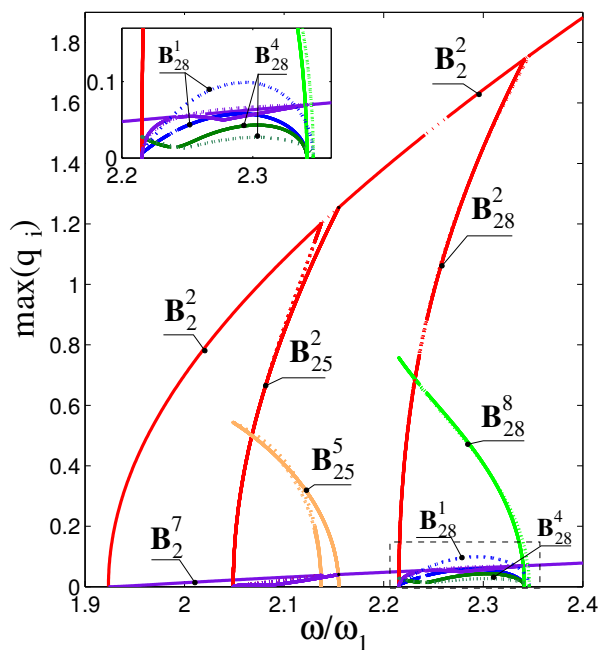
Figure 2: Frequency-amplitude dependence of the second mode of the selected plate. Maximum of modal coordinates q_i is plotted as a function of the normalised frequency ω/ω_1. q_2 in red, q_1 in blue, q_4 in dark green, q_5 in orange, q_7 in violet and q_8 in light green. Unstable states are displayed in a dotted line.

vestigation of wave turbulence in elastic materials [13].

References

[1] M. Amabili. Nonlinear vibrations of rectangular plates with different boundary conditions: theory and experiments. *Computers and Structures*, 82(31-32):2587–2605, 2004.

[2] G. Anlas and O. Elbeyli. Nonlinear vibrations of a simply supported rectangular metallic plate subjected to transverse harmonic excitation in the presence of a one-to-one internal resonance. *Nonlinear Dynamics*, 30(1):1–28, 2002.

[3] S. Bilbao. A family of conservative finite difference schemes for the dynamical von kármán plate equations. *Numerical Methods for Partial Differential equations*, 24(1):193–216, 2008.

[4] F. Boumediene, L. Duigou, E.H. Boutyour, A. Miloudi, and J.M. Cadou. Nonlinear forced vibration of damped plates by an asymptotic numerical method. *Computers and Structures*, 87(23-24):1508–1515, 2009.

[5] H-N Chu and G. Herrmann. Influence of large amplitudes on free flexural vibrations of rectangular elastic plates. *Journal of Applied Mechanics*, 23, 1956.

[6] A. Leissa. *Vibration of plates*. Acoustical Society of America, 1993.

[7] W.L. Li. Vibration analysis of rectangular plates with general elastic support. *Journal of Sound and Vibration*, 273(3):619–635, 2003.

[8] P. Ribeiro. Nonlinear vibrations of simply-supported plates by the p-version finite element method. *Finite Elements in Analysis and Design*, 41(9-10):911–924, 2005.

[9] P. Ribeiro and M. Petyt. Geometrical non-linear, steady-state, forced, periodic vibration of plate, part i: model and convergence study. *Journal of Sound and Vibration*, 226(5):955–983, 1999.

[10] P. Ribeiro and M. Petyt. Geometrical non-linear, steady-state, forced, periodic vibration of plate, part ii: stability study and analysis of multimodal response. *Journal of Sound and Vibration*, 226(5):985–1010, 1999.

[11] I. C. Seo, J. M. Lee, A. K. Bajaj, and C. M. Krousgrill. Subharmonic responses in harmonically excited rectangular plates with one-to-one internal resonance. *Chaos Solitons Fractals*, 8(4):479–498, 1997.

[12] O. Thomas and S. Bilbao. Geometrically nonlinear flexural vibrations of plates: In-plane boundary conditions and some symmetry properties. *Journal of Sound and Vibration*, 315(3):569–590, 2008.

[13] C. Touzé, S. Bilbao, and O. Cadot. Transition scenario to turbulence in thin vibrating plates. *Journal of Sound and Vibration*, 331(2):412–433, 2011.

[14] C. Touzé, S. Bilbao, L. Longo-Mucciante, O. Cadot, and A. Boudaoud. Vibrations chaotiques de plaques minces: application aux instruments de type cymbale. In *Proceedings of CFA 2010, 10eme Congrès Français d'Acoustique*, Lyon, April 2010.

[15] N. Yamaki. Influence of large amplitudes on flexural vibrations of elastic plates. *Zeitschrift für Angewandte Mathematik und Mechanik*, 41(12):501–510, 1961.